Eur. Phys. J. A (2018) **54**: 218
DOI 10.1140/epja/i2018-12655-6

THE EUROPEAN PHYSICAL JOURNAL A

Regular Article – Theoretical Physics

Reproducing heavy-ion fusion cross sections at extreme sub-barrier energies with a simple formula

Analysis of fusion hindrance with a Gaussian barrier distribution

C.L. Jiang[1,a], K.E. Rehm[1], B.B. Back[1], A.M. Stefanini[2], and G. Montagnoli[3]

[1] Physics Division, Argonne National Laboratory, 9700 S. Cass Avenue, Argonne, IL 60439, USA
[2] INFN, Laboratori Nazionali di Legnaro, I-35020 Legnaro (Padova), Italy
[3] Dipartimento di Fisica e Astronomia, Università di Padova, and INFN, Sez. di Padova, I-35131 Padova, Italy

Received: 4 October 2018 / Revised: 16 November 2018
Published online: 17 December 2018

Communicated by P. Capel

Abstract. Heavy-ion fusion hindrance occurs at extreme sub-barrier energies. This behavior is well reproduced with a simple cross section formula, which was developed by Siwek-Wilczynska *et al.*, based on a single-Gaussian distribution of fusion barrier heights, before the discovery of the hindrance phenomenon. This expression has not yet been widely used and referenced in the literature. An analysis by using this simple formula is presented for 29 systems, from ^{16}O + ^{18}O to ^{64}Ni + ^{124}Sn, all being measured down to less than 10 μb. The agreement with the data is even better than the ones from sophisticated Coupled-channels calculations. This simple expression also applies to fusion reactions in lighter systems. The three parameters contained in this formula vary in a relatively smooth fashion over the whole mass range, and can be used to extrapolate cross sections or to obtain an estimate of the excitation function for systems which have not been measured. Extensions and restrictions of this method are also discussed.

1 Introduction

Fusion is a complex process between two heavy nuclei. At energies above the barrier, fusion makes up the dominant part of the nuclear reaction cross section and is the main process to produce nuclei outside the valley of beta stability. At low energies the fusion cross sections decrease exponentially, even more rapidly than many other reaction channels. This behavior of fusion excitation functions introduces important ramifications in other fields, such as astrophysics.

The overall description and understanding of the heavy-ion fusion excitation function, covering the whole energy range from high above the Coulomb barrier down to the extreme sub-barrier region, becomes an important issue in reaction theory studies.

Measurements and analyses of fusion enhancements [1, 2], angular momentum distributions [3], fusion barrier distributions [4–7], and recently, the heavy-ion fusion hindrance [8–11], have been studied over the last sixty years. Coupled-Channels (CC) calculations have been developed as an elaborate and commonly accepted theoretical approach for describing heavy-ion reactions including fusion [12–14]. Many review articles of fusion reactions can be found in the literature. Some recent ones are listed in [7, 10, 11, 14], where references to earlier studies can be found.

There are two simple, analytic expressions of heavy-ion fusion excitation functions which have been commonly referenced and used. The black-body model [15] is based on the assumption that the collision energy must exceed a single fusion barrier, whereas the Wong formula [16] also allows for quantum mechanical tunneling through the barrier represented by a simple parabolic shape.

In 2002, Siwek-Wilczynska *et al.*, [17, 18] obtained a surprisingly simple, but accurate description of the fusion cross section based on a single-Gaussian distribution, $D_g(B)$, of fusion barrier heights [4, 19]

$$D_g(B) = \frac{1}{\sqrt{2\pi}W_g} \exp\left[-\left(\frac{B-V_g}{\sqrt{2}W_g}\right)^2\right]. \quad (1)$$

with

$$\sigma(E) = \frac{\pi R^2}{E}\int_{E_0}^{E}(E-B)D(B)\mathrm{d}B. \quad (2)$$

Here, V_g is the centroid of the barrier distribution and W_g the standard deviation of the distribution. The lower integration limits are $E_0 = -Q$ or 0, depending on whether

[a] e-mail: jiang@phy.anl.gov

the fusion Q value is negative or positive. In this case one obtaines another simple, analytic function for the cross section which includes the complementary error function erfc(Z)

$$\sigma_g(E) = \frac{\sqrt{\pi} R_g^2 W_g}{\sqrt{2}E} \left[\sqrt{\pi} Z \,\mathrm{erfc}(-Z) + \exp(-Z^2)\right], \quad (3)$$

with $Z = (E - V_g)/\sqrt{2}W_g$ and R_g the barrier radius[1].

This simple formula can reproduce the heavy-ion fusion excitation functions quite well. In ref. [18] a table was included for 46 systems heavier than ^{48}Ca+^{48}Ca. The data analysed in ref. [18] were mostly in the cross section range from 0.1 to 1000 mb. In fact, this formula has not been widely used and referenced in the literature.

At about the same time, heavy-ion fusion hindrance at extreme sub-barrier energies was discovered [8, 9, 20]. It was observed that the excitation functions for the systems ^{60}Ni + ^{89}Y [8] and ^{64}Ni + ^{64}Ni [20] at low energies decrease much faster than the predictions of CC calculations with standard Woods-Saxon potential. A large number of refined measurements have been performed since then, where the measured cross sections have been extended down to the nb level.

There is an excellent signature of this hindrance phenomenon in the form of a maximum that appears in the astrophysical S factor at extreme sub-barrier energies ($S(E) = E\sigma \exp(2\pi\eta)$, where $\eta = Z_1 Z_2 e^2/\hbar v$ is the Sommerfeld parameter). This phenomenon cannot be described by the CC calculations with a standard Woods-Saxon potential. It was soon realized that since the fusion Q values for fusion reactions in medium-mass or heavy systems are always negative, there must be an S-factor maximum due to energy conservation [9]. For fusion in lighter-mass systems, no such restriction exists since the fusion Q values are often positive. Whether there is also an S-factor maximum for these systems becomes an important question, since reliable extrapolations of excitation functions are especially important in nuclear astrophysics, where in many cases the existing technologies do not allow measurements of the fusion cross sections at the required low energies. For a theoretical description, it was found that the hindrance at low energy can be described by the saturation property or incompressibility of nuclear matter, and has been reproduced by refined CC calculations including a repulsive core [21,22] or a damping of the coupling strength inside the Coulomb barrier [23–25]. There are other suggestions to interpretate the deep sub-barrier fusion hindrance, in addition to the ones mentioned in ref. [10], such as the decoherence [26], dissipation [27,28], Pauli repulsion [29], DCTDHF calculations [30, 31] and the use of the proximity formalism [32].

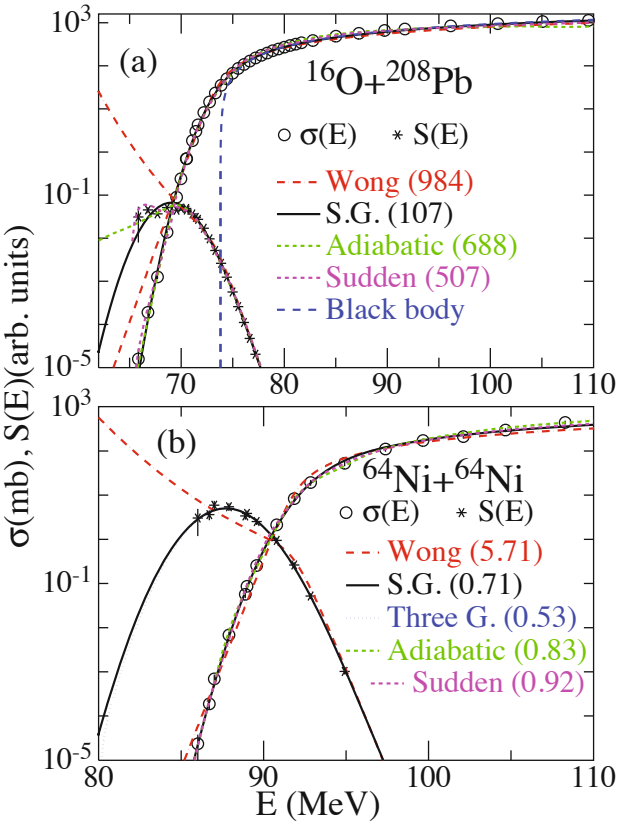

Fig. 1. Fusion cross sections, $\sigma(E)$, and the corresponding S factors, $S(E)$ for the systems ^{16}O+^{208}Pb [26,33] (panel a) and ^{64}Ni + ^{64}Ni [20] (panel b). See text for details.

2 Comparison with experimental data

Using eq. (3) for $\sigma_g(E)$, one can perform a least-squares fit to the experimental excitation function and obtain the parameters R_g, V_g and W_g that describe the barrier distribution and the fusion cross sections.

As a first example, we discuss the system ^{16}O + ^{208}Pb (shown in fig. 1(a)), where high-precision data measured in small energy steps and covering cross sections from 10^{-5} mb to 10^3 mb are available [26, 33]. The cross sections and the S factor are shown in fig. 1(a). For this system a clear maximum in $S(E)$ is observed. The blue dashed and red dot-dashed lines are the results from the black-body and the Wong formula, respectively. The latter shows good agreement with the data down to cross sections of about 0.1 mb, but overpredicts the data at the lowest energies by more than a factor of 10 and cannot reproduce the maximum of the S factor. Coupled-channels calculations with the sudden [21, 22] (magenta curve) or

[1] Equation (3) is an approximated form under the assumption that $(V_g - E_0)/\sqrt{2}W_g > 6$, which is valid for all cases of the present study. For very heavy system, the value of $(V_g - E_0)/\sqrt{2}W_g$ is smaller but still positive, eq. (3) should be taken as

$$\sigma_g(E) = \frac{\pi R_g^2 W_g Z}{\sqrt{2}E} \left[\mathrm{erf}(Z) - \mathrm{erf}(Z_0)\right] + \frac{\sqrt{\pi} R_g^2 W_g}{\sqrt{2}E} \left[\exp(-Z^2) - \exp(-Z_0^2)\right]. \quad (4)$$

Here $Z_0 = (E_0 - V_g)/\sqrt{2}W_g$, and erf($Z$) is the error function.

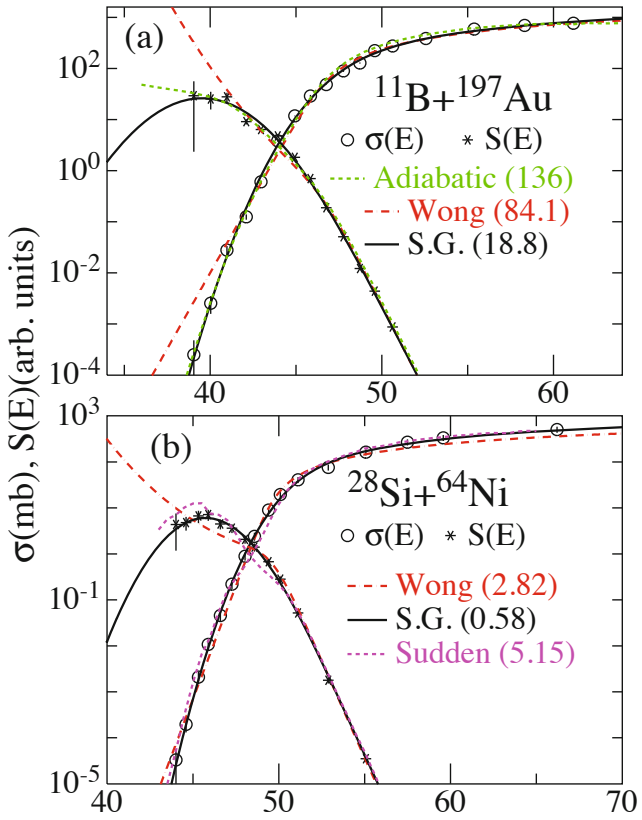

Fig. 2. Fusion cross sections, $\sigma(E)$, and the corresponding S factors, $S(E)$ for the systems $^{11}\mathrm{B}+{}^{197}\mathrm{Au}$ [34] (panel a) and $^{28}\mathrm{Si}+{}^{64}\mathrm{Ni}$ [35] (panel b).

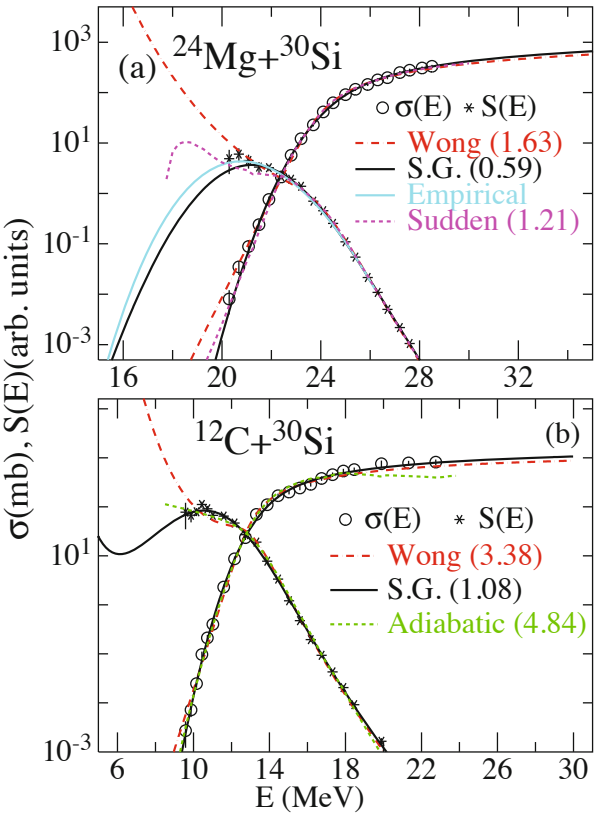

Fig. 3. Fusion cross sections, $\sigma(E)$, and the corresponding S factors, $S(E)$ for the systems $^{24}\mathrm{Mg}+{}^{30}\mathrm{Si}$ [36,37] (panel a) and $^{12}\mathrm{C}+{}^{30}\mathrm{Si}$ [38,39] (panel b).

the adiabatic model [23–25] (green curve), which include coupling to inelastic excitations and transfer reactions, are both reproducing the S-factor maximum and are in excellent agreement with the data over the whole energy range. It is interesting to note, however, that the use of the simple formula eq. (3) (black curve in fig. 1) gives an even better agreement with the data in a cross section range covering 8 orders of magnitude, as judged by the χ^2 value defined by

$$\chi^2 = \frac{1}{N-M}\sum_{i=1}^{N}\left((\sigma_i - \sigma_{\mathrm{exp}-i})\Big/\Delta\sigma_{\mathrm{exp}-i}\right)^2. \quad (5)$$

Here, σ_i and $\sigma_{\mathrm{exp}-i}$ are calculated and experimental cross sections, $\Delta\sigma_{\mathrm{exp}}$ are the experimental uncertainties, and N and M are the number of experimental data and adjustable parameters, respectively. The corresponding χ^2-values are included in parentheses in fig. 1. The number of free parameters for the Wong formula and for eq. (3) is $M = 3$. For the CC calculations, there are many adjustable parameters, related to the optical potential, and the nuclear structure of the individual channels. For simplicity, we also used $M = 3$, resulting in a lower limit for χ^2 for these calculations.

Fusion data of $^{64}\mathrm{Ni}+{}^{64}\mathrm{Ni}$ [20], $^{11}\mathrm{B}+{}^{197}\mathrm{Au}$ [34] and $^{28}\mathrm{Si}+{}^{64}\mathrm{Ni}$ [35] are shown in fig. 1(b), fig. 2(a) and fig. 2(b), respectively. These excitation functions all have been measured down to the nb level, and clear maxima appear in the S factor for $^{64}\mathrm{Ni}+{}^{64}\mathrm{Ni}$ and $^{28}\mathrm{Si}+{}^{64}\mathrm{Ni}$. Calculations with Wong's formula overpredict the yields at low energies. Both improved CC calculations (sudden model or adiabatic model) and fits using the single-Gaussian formula reproduce the S-factor maximium. It is important to note that the χ^2 value obtained by using the single-Gaussian distribution (S.G.) are always smaller than the ones obtained by CC calculations, including the adiabatic and sudden models.

The fusion Q values of the four systems are all negative: −46.48, −48.80, −5.04 and −8.20 MeV, respectively. As mentioned above, systems with positive fusion Q values, which are found in the lighter-mass region are of special interest. Two of them, $^{24}\mathrm{Mg}+{}^{30}\mathrm{Si}$ [36, 37] and $^{12}\mathrm{C}+{}^{30}\mathrm{Si}$ [38,39], measured recently at Legnaro, in normal and inverse kinematics, are shown in fig. 3(a) and 3(b), respectively. Their fusion Q values are 17.89 and 14.11 MeV. These results demonstrate that eq. (3) can describe the light systems as well. It is also important to note that the S factors for these two positive fusion Q-value systems appear to develop a maximum at extreme sub-barrier energy regions although more data points are needed to make a definite conclusion. Both the simple formula and CC calculations can reproduce the maxima, but the simple formula gives a superior fit to the data.

3 Logarithmic derivative

Since the hindrance phenomenon results in a steeper fall off of the excitation function, a representation in terms of the logarithmic derivative, $L(E) = \mathrm{d}(E\sigma(E))/\mathrm{d}E$ has been introduced [8, 9]. This representation does not depend on the absolute value of cross sections and is very sensitive to the shape of the excitation function. It was found that, an S-factor maximum appears at the crossing energy, E_s if the experimental $L(E)$ crosses the curve, given by the constant S factor, $L_{cs}(E) = \pi\eta(E)/E$. Empirical formulae, which can describe the heavy-ion fusion excitation function at low energies and can be used to extrapolate the data to lower energies, have been developed in refs. [40] and [41]. These formulae are

$$L(E) = A_0 + \frac{B_0}{E^{3/2}}, \quad \text{when } Q > 0, \tag{6}$$

or

$$L(E) = A_0 + \frac{B_0}{(E+Q)^{3/2}}, \quad \text{when } Q < 0. \tag{7}$$

Here, A_0 and B_0 are parameters obtained from least-squares fits to the experimental data at low energies and Q is the fusion Q value. The corresponding expressions for the cross section are

$$\sigma(E) = \sigma_s \frac{E_s}{E} \exp\left(A_0(E-E_s) - \frac{2B_0}{\sqrt{E_s}}\left[\sqrt{\frac{E_s}{E}} - 1\right]\right), \quad \text{when } Q > 0. \tag{8}$$

or

$$\sigma(E) = \sigma_s \frac{E_s}{E} \exp\left(A_0(E-E_s) - \frac{2B_0}{\sqrt{E_s+Q}}\left[\sqrt{\frac{E_s+Q}{E+Q}} - 1\right]\right), \quad \text{when } Q < 0. \tag{9}$$

Here σ_s, the cross section at the energy of S-factor maximum, E_s, is a fit parameter.

From eq. (3), the expression for the logarithmic derivative of the single-Gaussian formula can be obtained as

$$L_g(E) = \frac{1}{\sqrt{2}W_g} \frac{1+\mathrm{erf}(Z)}{Z(1+\mathrm{erf}(Z)) + \exp(-Z^2)/\sqrt{\pi}}, \tag{10}$$

with $Z = (E - V_g)/\sqrt{2}W_g$. The logarithmic derivative for the Wong formula is

$$L_w(E) = \frac{\hbar\omega}{2\pi} \frac{\exp(X)}{(1+\exp(X))\ln(1+\exp(X))}, \tag{11}$$

with $X = 2\pi(E - V_w)/\hbar\omega$.

The experimental logarithmic derivatives (symbols), constant S factor $L_{cs}(E)$ (green dashed lines) and the fitted $L(E)$ (black lines) for the systems ^{16}O + ^{208}Pb, ^{64}Ni + ^{64}Ni and ^{12}C + ^{30}Si are shown in figs. 4(a), 4(b) and 4(c), respectively. Results from the Wong formula (blue dash-dotted curves) are also shown. Around the crossing points between the experimental $L(E)$ and the constant S-factor curves $L_{cs}(E)$ at E_s, the calculations of eq. (10) are very similar to the empirical results of eqs. (8) and (9). The energies E_s of the S-factor maxima obtained from eq. (3) for these three systems are 69.06, 87.70 and 10.54 MeV, respectively, and agree well with the experimentally observed values, 68.4 ± 2.4, 87.5 ± 0.9 and 10.5 ± 0.5 MeV. This comparison demonstrates that the single-Gaussian barrier distribution gives the right behavior of the logarithmic derivative at low energies to describe the hindrance phenomenon in the measured energy region. The results of the Wong formula, on the contrary, are quite different; the logarithmic derivatives saturate at lower values, and fail to reproduce the data at low energies. The CC calculation result (sudden model) for the system ^{16}O + ^{208}Pb is also shown in fig. 4. The empirical extrapolations from eq. (6) for the system ^{24}Mg + ^{30}Si are shown as the light-blue curve in fig. 3 for comparison.

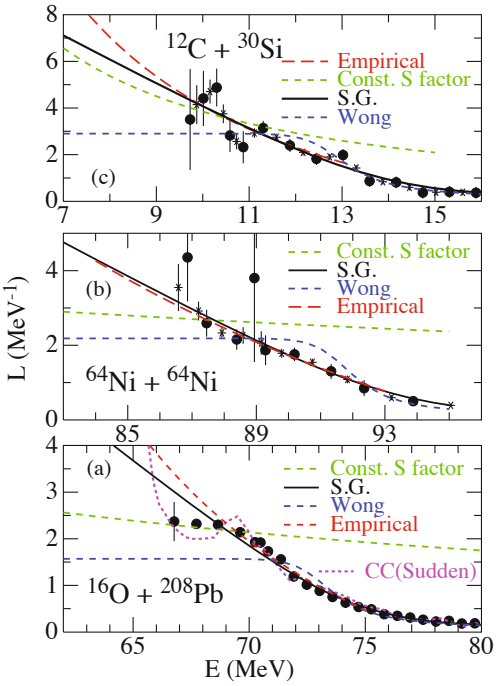

Fig. 4. Experimental logarithmic derivatives $L(E)$ (symbols) for the fusion reactions, ^{16}O + ^{208}Pb (a), ^{64}Ni + ^{64}Ni (b) and ^{12}C + ^{30}Si (c), in comparison with various calculations (see text for details).

4 Systematics of parameters and its application

The fusion cross sections calculated by eq. (3) give an excellent description of the data for a variety of systems; a summary of the fit parameters R_g, V_g and W_g is presented in table 1 for 29 systems, ranging from ^{16}O + ^{18}O

Table 1. Parameters R_g, V_g, and W_g obtained by least-squares fits for 29 fusion systems, whose lowest measured cross sections are less than 0.01 mb. Q is the fusion Q value, N is the number of data points in the fitting, χ^2 is the value defined in eq. (5), EVR and FF are cross sections for fusion-evaporation residues and fusion-fission, V_0 and R_0 are values obtained from eqs. (12) and (13), respectively. If different data sets are available for a given system, the most recent one was used for the least-squares fit.

System	Q	Type	N	data range	χ^2	R_g	V_g	W_g	V_0	R_0	ref.
	MeV			mb–mb		fm	MeV	MeV	MeV	fm	
$^{16}O + ^{18}O$	24.41	EVR	21	0.006–224	0.38	7.95±0.28	9.89±0.07	0.873±0.019	12.45	7.40	[42]
$^{12}C + ^{30}Si$	14.11	EVR	22	0.0027–815	1.08	7.79±0.19	13.31±0.07	0.962±0.023	15.57	7.77	[38,39]
$^{24}Mg + ^{30}Si$	17.89	EVR	20	0.0080–332	0.59	8.19±0.14	24.05±0.06	1.05±0.02	28.04	8.63	[36,37]
$^{6}Li + ^{198}Pt$	8.53	EVR	10	0.00017–348	45.7	7.89±0.34	27.43±0.24	1.75±0.09	30.61	11.01	[43]
$^{7}Li + ^{198}Pt$	8.82	EVR	11	0.0002–1004	5.93	9.71±0.12	28.04±0.08	1.65±0.02	30.23	11.15	[44]
$^{28}Si + ^{28}Si$	10.92	EVR	21	0.00063–453	0.99	9.11±0.61	29.54±0.25	1.50±0.07	32.27	8.75	[45]
$^{28}Si + ^{30}Si$	14.30	EVR	17	0.0044–500	0.97	7.92±0.32	28.13±0.12	1.16±0.04	31.90	8.85	[45,46]
$^{27}Al + ^{45}Sc$	9.63	EVR	16	0.00031–596	0.68	7.11±0.31	37.68±0.15	1.42±0.04	41.64	9.44	[47]
$^{32}S + ^{48}Ca$	7.66	EVR	21	0.0008–490	8.63	8.55±0.13	42.82±0.12	1.64±0.05	47.00	9.81	[48]
$^{36}S + ^{48}Ca$	7.55	EVR	25	0.0006–973	3.26	10.00±0.06	41.97±0.05	1.11±0.02	46.13	9.99	[49]
$^{11}B + ^{197}Au$	−5.00	EVR+FF	17	0.0003–770	18.8	10.56±0.21	46.81±0.13	1.78±0.06	49.11	11.58	[34]
$^{12}C + ^{198}Pt$	−13.96	EVR+FF	20	0.0001–670	12.5	10.89±0.27	55.38±0.13	1.81±0.04	57.65	11.69	[44]
$^{40}Ca + ^{40}Ca$	−14.18	EVR	21	0.0027–531	5.23	9.93±0.15	53.10±0.08	1.15±0.04	58.48	9.85	[50]
$^{40}Ca + ^{48}Ca$	4.56	EVR	23	0.0013–463	6.30	8.31±0.10	51.86±0.10	1.64±0.05	56.70	10.16	[51]
$^{48}Ca + ^{48}Ca$	−2.99	EVR	27	0.0006–506	7.43	9.87±0.10	51.17±0.05	1.08±0.03	55.03	10.47	[52,53]
$^{28}Si + ^{64}Ni$	−1.79	EVR	16	0.00003–506	0.58	8.05±0.26	50.45±0.11	1.40±0.03	55.71	10.13	[35]
$^{16}O + ^{208}Pb$	−46.48	EVR+FF	38	0.000016–1133	106	10.43±0.08	73.59±0.05	1.57±0.02	77.68	12.16	[26,33]
$^{54}Fe + ^{58}Ni$	−5.40	EVR	25	0.0011–433	24.2	9.13±0.15	91.51±0.14	1.76±0.07	95.16	11.02	[54]
$^{64}Ni + ^{64}Ni$	−48.80	EVR	16	0.00002–442	0.71	8.86±0.21	92.62±0.11	1.45±0.03	98.00	11.52	[20]
$^{40}Ca + ^{96}Zr$	−41.09	EVR	62	0.0027–474	5.67	9.63±0.37	94.15±0.05	2.95±0.03	100.01	11.52	[55]
$^{40}Ar + ^{112}Sn$	−77.20	EVR+FF	15	0.0084–478	4.16	9.19±0.18	104.40±0.18	2.45±0.08	109.22	11.87	[56]
$^{40}Ar + ^{116}Sn$	−73.11	EVR+FF	14	0.0038–512	9.75	8.99±0.35	103.84±0.27	2.44±0.10	108.47	11.95	[56]
$^{40}Ar + ^{122}Sn$	−64.96	EVR+FF	17	0.0018–661	8.97	9.90±0.24	103.79±0.21	2.66±0.08	107.40	12.07	[56]
$^{40}Ar + ^{144}Sm$	−105.77	EVR+FF	11	0.0016–322	6.85	8.20±0.43	124.49±0.31	2.29±0.10	128.85	12.47	[56]
$^{40}Ar + ^{148}Sm$	−96.37	EVR+FF	12	0.0008–353	7.26	9.16±0.59	125.60±0.53	3.51±0.16	128.14	12.54	[56]
$^{40}Ar + ^{154}Sm$	−83.10	EVR+FF	15	0.0016–407	24.4	8.38±0.60	122.80±0.73	4.17±0.24	127.11	12.64	[56]
$^{86}Kr + ^{76}Ge$	−90.14	EVR	15	0.0068–347	14.6	8.08±0.31	129.95±0.39	2.94±0.17	133.18	12.46	[57]
$^{58}Ni + ^{124}Sn$	−112.30	EVR+FF	15	0.00046–570	1.05	8.51±0.34	156.92±0.38	3.45±0.12	158.06	12.76	[58,59]
$^{64}Ni + ^{124}Sn$	−117.51	EVR+FF	17	0.0008–605	1.71	7.86±0.47	154.02±0.47	2.59±0.15	155.79	12.94	[58,59]

to $^{64}Ni + ^{124}Sn$, whose lowest measured cross sections are below 10 μb, and covering a cross section range of at least five orders of magnitude. The fusion Q value, the lowest and highest cross sections of the data set, and the χ^2 value are also listed. For fusion between heavy nuclei only those systems are included, where cross sections for the formation of evaporation residues (EVR) as well as for fusion fissions (FF) are available.

The parameters R_g, V_g and W_g obtained from the single-Gaussian analysis exhibit smooth behaviors when they are plotted in fig. 5 as a function of the Coulomb barrier calculated by

$$Z_P Z_T e^2 / \left[1.44\left(A_P^{1/3} + A_T^{1/3}\right)\right] \quad \text{(MeV)}. \qquad (12)$$

Here Z_P, A_P and Z_T, A_T are nuclear charge and mass number for projectile and target, respectively. The barrier radius parameter R_g is shown in fig. 5(a), normalized to the value

$$1.44\left(A_P^{1/3} + A_T^{1/3}\right) \quad \text{(fm)}. \qquad (13)$$

Figures 5(b) and 5(c) give the results of the average barrier height V_g and the barrier distribution width parameter W_g, normalized to the respective Coulomb barrier (eq. (12)). These parameters follow a general trend with superimposed fluctuations due to nuclear structure effects. This systematics may be used to make first-order predictions of fusion cross sections for unmeasured systems.

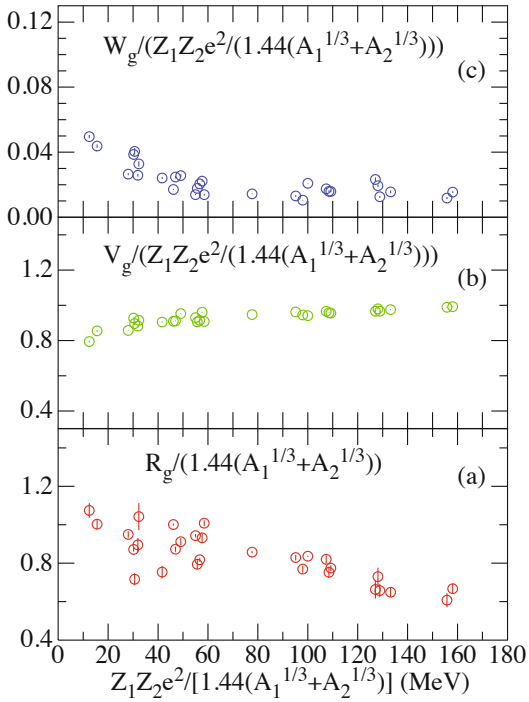

Fig. 5. Plots of the parameters R_g, V_g and W_g as function of the Coulomb barrier $Z_1Z_2e^2/[1.44(A_1^{1/3}+A_2^{1/3})]$ (MeV). In order to reduce the strong system-dependence, the parameters are scaled by known factors $1.44(A_1^{1/3}+A_2^{1/3})$ (fm) (eq. (12)) and $Z_1Z_2e^2/[1.44(A_1^{1/3}+A_2^{1/3})]$ (MeV) (eq. (13)). See text for details.

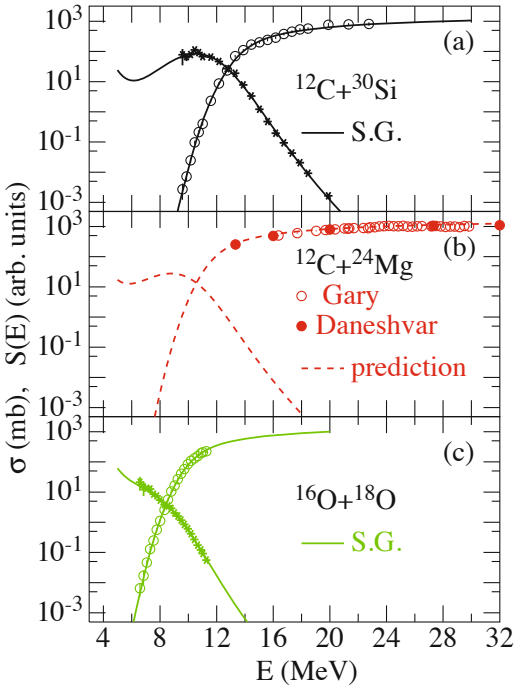

Fig. 6. Comparison for cross sections (mb) and S factors (arbitrary units) for fusion reactions ^{12}C+^{30}Si (a), ^{12}C+^{24}Mg (b) and ^{16}O + ^{18}O (c). The curve for ^{12}C + ^{24}Mg are predictions, while other curves are results of least-squares fits.

As an example, we have chosen the fusion of ^{12}C + ^{24}Mg. Experiments of fusion for ^{12}C+^{24}Mg have been performed by Daneshvar *et al.*, [60] and Gary *et al.*, [61], in the cross section range of 250–1200 mb and 500–1000 mb, respectively. This range is insufficient to obtain values for all three parameters of eq. (3). The cross sections and S factors measured for two neighboring systems ^{16}O+^{18}O [42] and ^{12}C+^{30}Si [38,39] are shown in figs. 6(a) and 6(c). The solid lines are the result of least-squares fits using eq. (3) with the parameters tabulated in table 1. While for ^{16}O + ^{18}O, no maximum in the S factor can be seen yet in the measured energy range, there are indications of an S factor maximum for ^{12}C + ^{30}Si at a c.m. energy of about 11 MeV. The interpolated values for the ^{12}C + ^{24}Mg system are $R_g = 7.88$, $V_g = 11.50$ and $W_g = 0.91$, with the predicted cross sections shown by the red dashed lines in fig. 6. It should be noted that, similar to the ^{12}C + ^{30}Si case, a maximum of the S factor is predicted to occur at a c.m. energy of about 9 MeV.

5 Extension and limitation

While the single-Gaussian barrier distribution (eq. (1)) provides an analytic formula (eq. (3)), which describes the experimental excitation functions for many systems, one may consider, whether there are other barrier distributions which can lead to even better results. Possible improvements for the barrier distribution given in eq. (1) include distributions with different widths on the high or low energy sides, a modification of the exponent in the Gaussian distribution or multi-component distributions. Test calculations show that this can lead to a considerable improvement in the calculated χ^2 values.

On the other hand, from previous studies of barrier distributions [7], it was found that some systems require a more complicated structure. The prime example for a multi-barrier distribution is the system ^{16}O+^{154}Sm. Since ^{154}Sm is deformed, there should be a range of Coulomb barriers depending on whether ^{16}O approaches ^{154}Sm at the long or the short axis [5, 6, 62–65]. The neighboring system ^{16}O + ^{144}Sm was also found to require an additional barrier at higher energies whose origin in a coupled-channels description was assigned to the excitation of a 3^- state in ^{144}Sm [5, 6, 64]. These results are rather different from the spectrum of the single-Gaussian distribution.

We have therefore investigated the choice of a multi-component barrier distributions to study the relation between structure and the improvements in χ^2 for the systems ^{16}O + ^{154}Sm and ^{16}O + ^{144}Sm.

The results of a CC description of fusion reactions between ^{16}O and the deformed nucleus ^{154}Sm [64, 65] are shown by the green dashed lines in fig. 7(a) (cross sections) and fig. 7(b) (barrier distribution). When compared to the single-Gaussian distribution (S.G., black curves), the CC results clearly shows two additional barrier components at the low-energy side of the main peak, which originate from different points of contact between ^{16}O and ^{154}Sm nuclei as discussed in ref. [5, 6, 64].

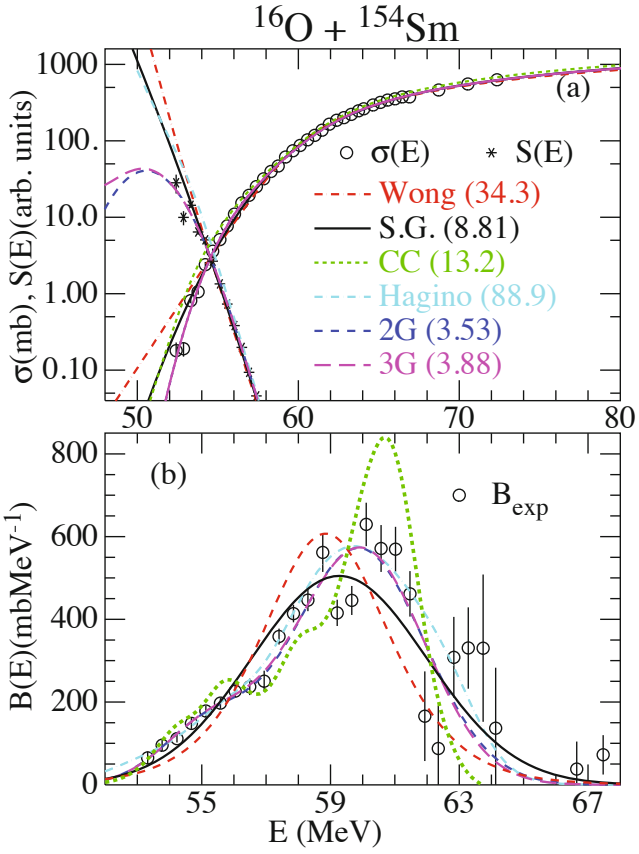

Fig. 7. Panel (a): cross sections (mb) and $S(E)$ factors (arbitrary units) for the fusion reaction $^{16}\mathrm{O} + ^{154}\mathrm{Sm}$ [5,6] are compared with theoretical predictions. The numbers in parentheses give the χ^2 values defined in eq. (5). Panel (b): comparison of the barrier distributions $B(E) = \pi R^2 D(E)$ used for describing the same fusion reaction.

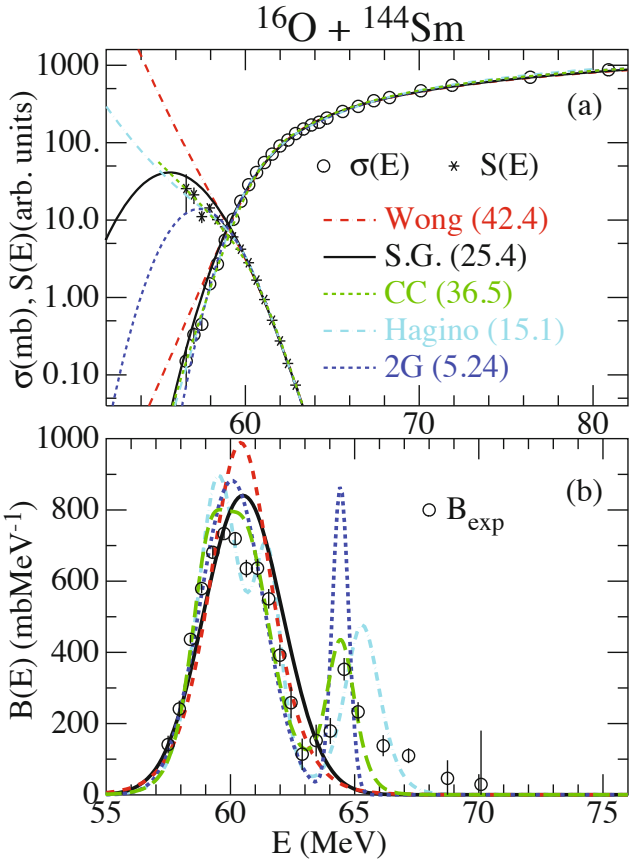

Fig. 8. Panel (a): cross sections (mb) and $S(E)$ factors (arbitrary units) for the fusion reaction $^{16}\mathrm{O} + ^{144}\mathrm{Sm}$ [5,6] are compared with theoretical predictions. The numbers in parentheses give the χ^2 values defined in eq. (5). Panel (b): comparison of the barrier distributions $B(E) = \pi R^2 D(E)$ used for describing the same fusion reaction.

Hagino *et al.* have recently developed a new method for obtaining the barrier distributions [66] by assuming that the excitation function is a sum of several components, each described by the Wong formula. The barrier distribution is then obtained by the second-derivative method (with $\Delta E = 1.8\,\mathrm{MeV}$) with the parameters optimized by a least-squares fit to the experimental barrier distribution $B_{\mathrm{exp}}(E)$. For the system $^{16}\mathrm{O} + ^{154}\mathrm{Sm}$, they obtained a 5-component distribution, shown by the cyan dashed line in fig. 7(b).

Least-squares fits with barrier distributions consisting of two- or three-Gaussian components (with 6 or 9 free parameters) are shown in fig. 7(b) by the blue dashed (2G) and magenta dashed (3G) lines. It is interesting to note that the three various barrier distributions given by the blue (two-Gaussians), cyan (Hagino) and green (CC) curves are quite different, especially on the high energy side, but result in similar excitation functions which are all close to the experimental data although with different χ^2 values.

Another example for a multi-barrier distribution can be found in the neighboring system $^{16}\mathrm{O} + ^{144}\mathrm{Sm}$ which is shown in fig. 8. A comparison of the different fusion barrier distributions used to describe this system is given in fig. 8(b). Contrary to the ^{154}Sm nucleus, where the deformation led to additional barrier components at low energies, the closed-shell nucleus ^{144}Sm requires an additional barrier at higher energies, whose origin was assigned to the excitation of a 3^- state in ^{144}Sm [5,6,64,65]. This additional peak at higher energies is also present in the analysis by Hagino *et al.* [66] with the method mentioned above, using three Wong components (cyan line in fig. 8(b)). It should also be mentioned that the additional high-energy peak in the barrier distribution calculated from the fusion excitation function is not observed in an analysis using the quasi-elastic scattering measurement (see ref. [11] and references therein). This was attributed to a reduced sensitivity of the quasi-elastic excitation functions at energies above the Coulomb barrier. The blue curve is again the result of a barrier distribution using two-Gaussians (2G) which also predicts an additional peak at higher energies. This peak in the distribution improves the χ^2 in the least-squares fits to the excitation function from 25 to 5, when compared to a single-Gaussian description. Using a three-Gaussian distribution improves the χ^2 only slightly and has not been included in the plot.

It should be noted that the S factors for the system $^{16}O + ^{154}Sm$ and $^{16}O + ^{144}Sm$ do not yet show a maximum in the energy region studied in the experiment. The lowest cross section measured in these two experiments is about 0.15 mb. Since the fusion Q values of the reaction $^{16}O + ^{144,154}Sm$ are negative, there has to be an S-factor maximum in the extreme sub-barrier region. Fits with a two-Gaussian distribution for $^{16}O + ^{154}Sm$ and a single- and two-Gaussian distribution for $^{16}O + ^{144}Sm$ predict an S-factor maximum at low energy as shown in figs. 7(a) and 8(a).

While the single-Gaussian parameterization is quite successful in describing a large number of fusion cross sections, it should also be emphasized that this formula as well as the method using the barrier distribution $D_{test}(E)$ (eq. (2)) cannot be applied to all fusion systems. From the definition of eq. (2), one can see that the excitation function is always a monotonic rising function. Thus, eqs. (1) and (2) cannot be used for a description of fusion reactions at higher energies, where deep-inelastic scattering and incomplete fusion can lead to a decrease of the fusion cross section. The same holds for lighter systems (*e.g.* $^{16}O+^{16}O$, $^{12}C+^{16}O$, $^{12}C+^{12}C$ etc.) where oscillations and resonance structures appear in the excitation functions.

Another limitation of this description originates from the use of the classical approximation (black body model, see refs. [4, 19]) which requires that $R/\lambda\!\!\!^{-} \gg 1$. Here R is the size of the fusion system and $\lambda\!\!\!^{-} = \lambda/2\pi$ with λ being the DeBroglie wavelength. Taking the values of R from fig. 5(a) and the $\lambda\!\!\!^{-}$ from the energy $V_g - 6(\sqrt{2}W_g)$ (the low end of the effective energy region), one obtaines $R/\lambda\!\!\!^{-}$ values for the systems listed in table 1, of about 11 and 8 for $^{12}C + ^{30}Si$ and $^{16}O + ^{18}O$, and between 25–170 for others. Thus the lightest system included in table 1 is the $^{16}O + ^{18}O$. For the system $^{12}C + ^{30}Si$ (shown in fig. 3(b)) we observe an increase in the calculated S factor for energies below 5 MeV. This behavior is also seen for $^{28}Si + ^{64}Ni$ if one expands the X-scale to very low energy. These may render the application and the extrapolation to low energies using the present prescription unreliable for systems lighter than $^{16}O + ^{18}O$.

6 Summary

The simple formula for describing fusion excitation functions based on the single-Gaussian barrier distribution has been used to reproduce the heavy-ion fusion hindrance at extreme sub-barrier energies. A quantitaive comparison with experimental data shows that the χ^2 values obtained with this formula are often smaller than the ones obtained by CC calculations (including the sudden model and the adiabatic model) or the Wong formula.

A study of 29 colliding systems, whose excitation functions have all been measured down to the 10 μb level, has been presented. The barrier distribution parameters, R_g, V_g and W_g for these systems show smooth trends superimposed with fluctuations caused by nuclear structure effects.

Better agreement with the data can be obtained by choosing a more elaborate formula for the barrier distribution, which, however, comes at the expense of additional adjustable parameters. A restriction for the application of the formula has also been noted.

The success of the present formula with a single Gaussian, together with the systematics of the parameters R_g, V_g and W_g, offer the possibity to use this formula to extrapolate cross sections, and to obtain an estimate of the excitation function for systems which have not yet been measured. An example has been shown for the system $^{12}C + ^{24}Mg$.

We want to thank K. Hagino for valuable discussions and A. Schrivastava, S. Mişisu and T. Ichikawa for providing us with some of the data shown in this publication. We also are grateful to H. Esbensen for his long-term collaboration that served to clarify the fusion phenomenon. This work was supported by the US Department of Energy, Office of Nuclear Physics, under Contract No. DE-AC02-06CH11357.

References

1. M.M. Beckerman *et al.*, Phys. Rev. Lett. **45**, 1472 (1980).
2. M.M. Beckerman, Phys. Rep. **129**, 145 (1985).
3. R. Vandenbosch, Annu. Rev. Nucl. Part. Sci. **42**, 477 (1992).
4. N. Rowley, G.R. Satchler, P.H. Stelson, Phys. Lett. B **254**, 25 (1991).
5. J.R. Leigh *et al.*, Phys. Rev. C **47**, 437 (1993).
6. J.R. Leigh *et al.*, Phys. Rev. C **52**, 3151 (1995).
7. M. Dasgupta, D.J. Hinde, N. Rowley, A.M. Stefanini, Annu. Rev. Nucl. Part. Sci. **48**, 401 (1998).
8. C.L. Jiang *et al.*, Phys. Rev. Lett. **89**, 052701 (2002).
9. C.L. Jiang, H. Esbensen, B.B. Back, R.V.F. Janssens, K.E. Rehm, Phys. Rev. C **69**, 014604 (2004).
10. B.B. Back, H. Esbensen, C.L. Jiang, K.E. Rehm, Rev. Mod. Phys. **86**, 317 (2014).
11. G. Montagnoli, A.M. Stefanini, Eur. Phys. J. A **53**, 169 (2017).
12. C.H. Dasso, S. Landowne, A. Winther, Nucl. Phys. A **405**, 381 (1983).
13. C.H. Dasso, S. Landowne, A. Winther, Nucl. Phys. A **407**, 221 (1983).
14. K. Hagino, N. Takigawa, Prog. Theor. Phys. **128**, 1061 (2012).
15. J.M. Blatt, V.F. Weisskopf, *Theoretical Nuclear Physics* (John Wiley and Sons, New York, 1952) p. 346.
16. C.Y. Wong, Phys. Rev. Lett. **31**, 766 (1973).
17. K. Siwek-Wilczynska, E. Siemaszko, J. Wilczynski, Acta Phys. Pol. B **33**, 451 (2002).
18. K. Siwek-Wilczynska, J. Wilczynski, Phys. Rev. C **69**, 024611 (2004).
19. P.H. Stelson *et al.*, Phys. Lett. B **205**, 190 (1988).
20. C.L. Jiang *et al.*, Phys. Rev. Lett. **93**, 012701 (2004).
21. S. Mişicu, H. Esbensen, Phys. Rev. Lett. **96**, 112701 (2006).
22. S. Mişicu, H. Esbensen, Phys. Rev. C **75**, 034606 (2007).
23. T. Ichikawa, K. Hagino, A. Iwamoto, Phys. Rev. C **75**, 057603 (2007).

24. T. Ichikawa, K. Hagino, A. Iwamoto, Phys. Rev. Lett. **103**, 202701 (2009).
25. T. Ichikawa, K. Matsuyanagi, Phys. Rev. C **88**, 011602(R) (2013).
26. M. Dasgupta *et al.*, Phys. Rev. Lett. **99**, 192701 (2007).
27. A. Diaz-Torres, Phys. Rev. **82**, 054617 (2010).
28. A. Diaz-Torres, Phys. Rev. C **78**, 064604 (2008).
29. C. Simenel, A.S. Umar, K. Godbey, M. Dasgupta, D.J. Hind, Phys. Rev. C **95**, 031601(R) (2017).
30. A.S. Umar, V.E. Oberacker, Phys. Rev. C **77**, 064605 (2007).
31. A.S. Umar, V.E. Oberacker, Eur. Phys. J. A **39**, 243 (2009).
32. O.N. Ghodsi, R. Gharei, Phys. Rev. C **88**, 054617 (2017).
33. C.R. Morton *et al.*, Phys. Rev. C **60**, 044608 (1999).
34. A. Shrivastava *et al.*, Phys. Rev. C **96**, 034620 (2017).
35. C.L. Jiang *et al.*, Phys. Lett. B **640**, 18 (2006).
36. A. Morsad, J.J. Kolata, R.J. Tighe, X.J. Kong, E.F. Aguilera, J.J. Vega, Phys. Rev. C **41**, 988 (1990).
37. C.L. Jiang *et al.*, Phys. Rev. Lett. **113**, 022701 (2014).
38. W.J. Jordan, J.V. Maher, J. Peng, Phys. Lett. **87**, 38 (1979).
39. G. Montagnoli *et al.*, Phys. Rev. C **97**, 04617 (2018).
40. C.L. Jiang *et al.*, Phys. Rev. C **75**, 015803 (2007).
41. H. Esbensen, C.L. Jiang *et al.*, Phys. Rev. C **79**, 064614 (2009).
42. J. Thomas, Y.T. Chen, S. Hinds, D. Meredith, M. Olson, Phys. Rev. C **13**, 1679 (1986).
43. A. Shrivastava *et al.*, Phys. Rev. Lett. **103**, 232702 (2009).
44. A. Shrivastava *et al.*, Phys. Lett. B **718**, 931 (2013).
45. G. Montagnoli *et al.*, Phys. Rev. C **90**, 044608 (2014).
46. C.L. Jiang *et al.*, Phys. Rev. C **78**, 017601 (2008).
47. C. Jiang *et al.*, Phys. Rev. C **81**, 024611 (2010).
48. G. Montagnoli *et al.*, Phys. Rev. C **87**, 014611 (2013).
49. A.M. Stefanini *et al.*, Phys. Rev. C **78**, 044607 (2008).
50. G. Montagnoli *et al.*, Phys. Rev. C **85**, 024607 (2012).
51. C.L. Jiang *et al.*, Phys. Rev. C **82**, 041601 (2010).
52. A.M. Stefanini *et al.*, Phys. Lett. B **679**, 95 (2009).
53. G. Montagnoli *et al.*, Phys. Rev. C **85**, 024607 (2012).
54. A.M. Stefanini *et al.*, Phys. Rev. C **82**, 014614 (2010).
55. A.M. Stefanini *et al.*, Phys. Lett. B **728**, 639 (2014).
56. W. Reisdorf *et al.*, Nucl. Phys. A **438**, 212 (1985).
57. W. Reisdorf *et al.*, Nucl. Phys. A **444**, 154 (1985).
58. K.T. Lesko *et al.*, Phys. Rev. C **34**, 2155 (1986).
59. C.L. Jiang *et al.*, Phys. Rev. C **91**, 044602 (2015).
60. K. Daneshar *et al.*, Phys. Rev. C **25**, 1342 (1982).
61. S. Gary, C. Volant, Phys. Rev. C **25**, 1877 (1982).
62. R.G. Stokstad, Y. Eisen, S. Kaplanis, D. Pelte, U. Smilansky, I. Tserruya, Phys. Rev. Lett. **41**, 465 (1978).
63. R.G. Stokstad, Y. Eisen, S. Kaplanis, D. Pelte, U. Smilansky, I. Tserruya, Phys. Rev. C **21**, 2427 (1980).
64. K. Hagino, N. Rowley, A.T. Kruppa, Comput. Phys. Commun. **123**, 143 (1999).
65. K. Hagino, CCFULL Home Page, `http://www.nucl.phys.tohoku.ac.jp/~hagino/ccfull.html`.
66. K. Hagino, Phys. Rev. C **93**, 061615 (2016).